Thermal Conductivity and Elastic Constants of PEDOT:PSS with High Electrical Conductivity

ARTICLE *in* MACROMOLECULES · JANUARY 2015

Impact Factor: 5.8 · DOI: 10.1021/ma502099t

6 AUTHORS, INCLUDING:

Jun Liu
North Carolina State University
13 PUBLICATIONS **167** CITATIONS
SEE PROFILE

Xiaojia Wang
University of Minnesota Twin Cities
17 PUBLICATIONS **227** CITATIONS
SEE PROFILE

Dongyao Li
University of Illinois, Urbana-Champaign
4 PUBLICATIONS **32** CITATIONS
SEE PROFILE

David G Cahill
University of Illinois, Urbana-Champaign
359 PUBLICATIONS **13,862** CITATIONS
SEE PROFILE

Macromolecules

Article

pubs.acs.org/Macromolecules

Thermal Conductivity and Elastic Constants of PEDOT:PSS with High Electrical Conductivity

Jun Liu,*[,†] Xiaojia Wang,[‡] Dongyao Li,[†,§] Nelson E. Coates,[∥,#] Rachel A. Segalman,[⊥] and David G. Cahill[†,§]

[†]Department of Materials Science and Engineering and Materials Research Laboratory, University of Illinois, Urbana, Illinois 61801, United States

[‡]Department of Mechanical Engineering, University of Minnesota, Minneapolis, Minnesota 55455, United States

[§]International Institute for Carbon Neutral Energy Research, Kyushu University, Fukuoka 819-0395, Japan

[∥]The Molecular Foundry, Materials Science Division, Lawrence Berkeley National Laboratory, Berkeley, California 94720, United States

[⊥]Department of Chemical Engineering, University of California, Santa Barbara, California 93106, United States

ABSTRACT: Mixtures of poly(3,4-ethylenedioxythiophene) and polystyrenesulfonate (PEDOT:PSS) have high electrical conductivity when cast from aqueous suspensions in combination with a high boiling-point cosolvent dimethyl sulfoxide (DMSO). The electronic component of the thermal conductivity of these highly conducting polymers is of interest for evaluating their potential for thermoelectric cooling and power generation. We find, using time-domain thermoreflectance measurements of thermal conductivity along multiple directions of thick (>20 μm) drop-cast PEDOT films, that the thermal conductivity can be highly anisotropic ($\Lambda_{\parallel} \approx 1.0$ W m^{-1} K^{-1} and $\Lambda_{\perp} \approx 0.3$ W m^{-1} K^{-1} for the in-plane and through-plane directions, respectively) when the electrical conductivity in the in-plane direction is large ($\sigma \approx 500$ S cm^{-1}). We relate the increase in thermal conductivity to the estimated electronic component of the thermal conductivity using the Wiedemann−Franz law, and find that our data are consistent with conventional Sommerfeld value of the Lorenz number. We use measurements of the elastic constants ($C_{11} \approx 11$ GPa and $C_{44} \approx 17$ GPa) of spin-cast PEDOT films and through-plane thermal conductivity ($\Lambda_{\perp} \approx 0.3$ W m^{-1} K^{-1}) of drop-cast and spin-cast films to support our assumption that the phonon contribution to the thermal conductivity does not change significantly with DMSO composition.

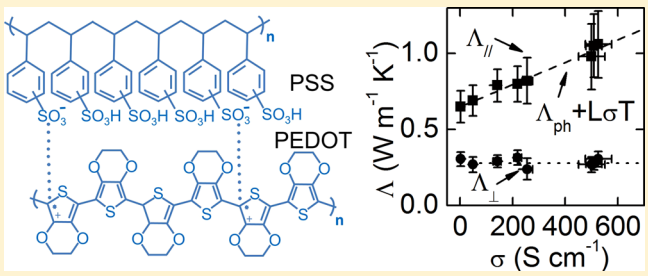

1. INTRODUCTION

Poly(3,4-ethylenedioxythiophene) (PEDOT) is an extensively studied conducting polymer due to its environmental stability, mechanical flexibility, low cost, tunable electrical conductivity, and solution processability.[1,2] Recently, mixtures of PEDOT and polystyrenesulfonate (PSS) have been found to have large electrical conductivity in the in-plane direction when cast from aqueous suspensions in combination with high boiling-point cosolvents such as dimethyl sulfoxide (DMSO), making PEDOT:PSS a promising candidate for applications in thermoelectric energy conversion.[3,4]

The efficiency of a thermoelectric material is characterized by the dimensionless figure of merit ZT[5]

$$\mathrm{ZT} = \frac{\sigma S^2 T}{\Lambda_e + \Lambda_{ph}} = \frac{S^2}{L}\left(\frac{\Lambda_e}{\Lambda_e + \Lambda_{ph}}\right) \quad (1)$$

where σ is the electrical conductivity, S is the Seebeck coefficient, T is the absolute temperature, Λ_e is the electronic component of the thermal conductivity, Λ_{ph} is the phonon contribution to the thermal conductivity, and L is the Lorenz number $L = \Lambda_e/(\sigma T)$. All other things being equal, a small value of the Lorenz number enhances ZT.

In metals and highly doped semiconductors, the electronic component of the thermal conductivity is typically proportional to the electrical conductivity following the prediction of the Wiedemann−Franz law (WFL) $\Lambda_e = L\sigma T$. The Lorenz number L is typically observed to be within 20% of the Sommerfeld value $L = 2.45 \times 10^{-8}$ W Ω K^{-2}.[6,7] Theoretical calculations show that the Lorenz number can be more significantly decreased when the bandwidth of the electron or hole dispersion is small.[8] Anomalously small values of the Lorenz number have been reported in calculations (e.g., in InGaAs/InGaAlAs superlattices[9]) and measurements (e.g., in Pt nanowires[10,11]). However, there have been few studies of conducting polymers to determine if the electronic component of the thermal conductivity is proportional to the electrical conductivity or if the Lorenz number is unusually small or large.

Received: October 13, 2014
Revised: January 12, 2015
Published: January 29, 2015

DOI: 10.1021/ma502099t
Macromolecules 2015, 48, 585−591

Salamon et al.[12] found that the WFL is valid in tetrathiafulvalene−tetracyanoquinodimethane (TTF−TCNQ) and the Lorenz number is close to the Sommerfeld value. Mermilliod et al.[13] reported that the increase of thermal conductivity in iodine-doped polyacetylene compared to that of a pristine polyacetylene is larger than what can be explained with an increase of the electronic thermal conductivity based on the Sommerfeld value of the Lorenz number.

In this work, thin (≈65 nm) spin-cast and thick (>20 μm) drop-cast PEDOT:PSS films are prepared with different electrical conductivities by systematically varying the concentration of the DMSO cosolvent. We use time-domain thermoreflectance (TDTR), an ultrafast laser-based pump−probe method,[14] to measure the thermal conductivity and heat capacity. We use picosecond acoustics and surface acoustic waves to measure the elastic constants. The major contribution of this work is that we find the changes of thermal conductivity as a function of electrical conductivity in PEDOT:PSS films are consistent with the WFL and the Sommerfeld value of the Lorenz number.

2. SAMPLE PREPARATION

The PEDOT:PSS aqueous solution (Clevious PH1000 purchased from Heraeus) containing ≈1 wt % PEDOT: PSS (1:2.5 weight ratio), was mixed with cosolvent DMSO (0−4 wt %). We used dynamic light scattering (DLS) to determine the average particle diameter in the as-received PEDOT: PSS aqueous dispersion, ≈19 nm. Preliminary samples were prepared at the Molecular Foundry; data reported in this paper were acquired on samples prepared at UIUC. Relatively thick films (>20 μm) were formed by drop-casting the DMSO-mixed PEDOT:PSS solution onto a polydimethylsiloxane (PDMS) substrate (Sylgard 184, Dow Corning) with a droplet diameter ≈2.5 cm. The droplet was then evaporated at 70 °C for ≈3 h in air. For simplicity, we refer to these DMSO-mixed PEDOT:PSS films as PEDOT films unless the DMSO composition is needed. The drop-cast PEDOT film was then peeled off the PDMS substrate and cut into three pieces: (i) a square piece from the central part (≈0.6 cm × 0.6 cm × 25 μm), where the film thickness is relatively uniform, for electrical conductivity measurement; (ii) a piece (≈0.6 cm × 1.0 cm × 30 μm) for through-thickness thermal conductivity measurement; and (iii) a piece (≈0.2 cm × 0.5 cm × 40 μm) to embed in epoxy matrix for measuring the in-plane thermal conductivity.

We used the same procedure for embedding the PEDOT film in an epoxy matrix as described in our previous work on polymer fibers.[15] The cross-sectional PEDOT film surface was then prepared by dry-cutting the epoxy matrix parallel to the cross-sectional PEDOT film direction using diamond blade ultramicrotomy (Leica EM UC6). We start the cutting with a large feed (1 μm) and a fast speed (200 mm/s) and then gradually change the conditions to a small feed (30 nm) and a slow speed (30 mm/s). During the dry-cutting, the PEDOT sections are constantly removed by compressed air to keep the blade clean.

Relatively thin PEDOT films (≈65 nm or ≈140 nm) were spin-cast on a Si substrate with either ≈10 nm or ≈315 nm thermally grown oxides. To improve the uniformity of the spin-cast layers, the DMSO-mixed PEDOT:PSS aqueous solution was sonicated for 20 min and filtered by a syringe filter (0.2 μm pore-size, Nylon membrane) prior to spin-casting at 4000 rpm for 40 s. The sample was annealed on a hot plate at 130 °C for 15 min after each layer was spin-cast. PEDOT thin films with thickness of ≈65 nm and ≈140 nm were obtained by spin-coating once and three times, respectively.

The thickness of drop-cast PEDOT films d was measured by profilometry; the thickness of spin-cast PEDOT films d was measured by tapping-mode atomic force microscopy (AFM). The rms surface roughness derived from AFM measurements over a 15 × 15 μm^2 area are 3−6 nm for drop-cast cross-sectional microtomed PEDOT films, ≈7 nm for the surface of drop-cast PEDOT films, and ≈5 nm for spin-cast PEDOT films. This satisfies the requirements of TDTR measurements, where typically an rms roughness of <15 nm is sufficient to avoid artifacts created by thermoelastic effects that modulate the intensity of diffuse light scattering.[16]

3. MEASUREMENTS

3.1. Electrical Conductivity. The in-plane electrical sheet resistance of drop-cast and spin-cast PEDOT films was measured by a four-point probe station specially designed for measuring soft materials. The homemade circuit box places the sample film in series with a reference resistor. The voltage drops across the sample film and series resistor were measured using a high-impedance multimeter. The probe tip radius is 25 μm and the force on each tip is ≈0.4 N. Since the PEDOT films have a finite area (≈6 × 6 mm^2 for drop-cast films and ≈10 × 10 mm^2 for spin-cast films) compared to the tip spacing (≈1 mm), a correction factor is applied to the measured resistance.[17] At least five measurements were done on the electrical resistance of each sample. The error bars are calculated by taking into account the uncertainty in the film thickness and the uncertainty in the multiple measurements of electrical resistance.

3.2. Thermal Conductivity. Prior to the TDTR measurements, Al thin films were deposited on the samples by magnetron sputtering. In TDTR, a mode-locked Ti:sapphire laser produces a train of pulses at a repetition rate of 80 MHz. A mechanical delay stage is used to change the optical path difference between the pump and probe before they are focused through an objective lens onto the sample surface. The pump beam is modulated at frequency f so that the thermoreflectance change at the sample surface can be detected by the probe beam through lock-in detection. Further details on TDTR can be found elsewhere.[14,16,18]

We used frequency-dependent TDTR[18−20] to measure both the thermal conductivity Λ and heat capacity C of spin-cast films. This approach is based on the fact that the sensitivities of the measurement signal to Λ and C vary differently with f. At relatively high f, the film thickness d is usually much larger than the thermal penetration depth in the sample $L = (\Lambda/\pi C f)^{1/2}$[14] ($d \gg L$); in this case, the thermal effusivity of the film $(\Lambda C)^{1/2}$ governs the heat flow in the sample. At sufficiently low f, $d \ll L$, the thermal resistance d/Λ governs the heat flow in the sample and the signal is more sensitive to Λ and less sensitive to C. For intermediate modulation frequencies, the sensitivity of the measurement signal to C crosses through zero.

We measured thin DMSO-mixed PEDOT spin-cast films (≈65 nm) with different DMSO compositions on a Si substrate with ≈10 nm thermal oxide at three modulation frequencies, 2.0, 3.4, 9.8 MHz, with a $1/e^2$ radius of the focused laser beams of w_0 = 11.7 μm. For each sample, we simultaneously fit the TDTR ratio data at the three modulation frequencies to extract Λ and C of the PEDOT thin films. In the fitting, the heat capacities of Al and Si are adopted from literature values.[21,22] The thickness of Al thin film was obtained from picosecond

DOI: 10.1021/ma502099t
Macromolecules 2015, 48, 585−591

acoustics using a longitudinal speed of sound 6.42 nm/ps.[23] The thermal conductivity of the Al thin film was calculated using the WFL and the electrical resistance of the same transducer layer deposited on a ≈315 nm SiO_2 on Si reference sample.

To validate our measurement approach, a ≈100 nm-thick poly(methyl methacrylate) (PMMA) film was spin-cast on a silicon substrate and measured using a similar approach. The best-fit values are $\Lambda = 0.18 \pm 0.02$ W m^{-1} K^{-1} and $C = 1.7 \pm 0.2$ J cm^{-3} K^{-1}, and the difference is within 5% as compared with the reported values of PMMA[24,25]

Figure 1 shows the geometry of TDTR measurements of through-plane and in-plane thermal conductivity of drop-cast

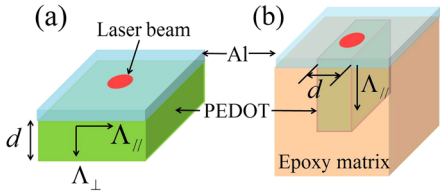

Figure 1. Schematic diagrams of TDTR measurements of through-plane and in-plane thermal conductivity of drop-cast DMSO-mixed PEDOT:PSS films with a thickness d. Aluminum thin films are deposited on the samples by magnetron sputtering. (a) Sample configuration for measuring through-plane thermal conductivity $\Lambda_\perp$. The incident laser beam is perpendicular to the plane of film. (b) Sample configuration for measuring in-plane thermal conductivity $\Lambda_\parallel$: the film was embedded in an epoxy matrix as prepared by diamond blade microtomy. This sample was then oriented so that the direction of the incident laser beam is parallel to the original plane of the drop-cast film.

PEDOT films. Through-plane thermal conductivity of drop-cast PEDOT films $\Lambda_\perp$ was measured using TDTR at $f = 9.8$ MHz using a 5× objective lens ($w_0 = 11.7$ μm) and a sample configuration as shown in Figure 1a. The drop-cast PEDOT films are "thermally thick" under this measurement condition since $d \gg L$ ($d \approx 40$ μm and $L \approx 0.07$ μm). We assume the heat capacity of the drop-cast PEDOT films is the same as the spin-cast PEDOT films since these PEDOT samples were cast from the same DMSO-mixed PEDOT:PSS aqueous solution and should have similar spectra of vibrational modes.

To measure the in-plane thermal conductivity of the drop-cast PEDOT film $\Lambda_\parallel$, the film was embedded in an epoxy matrix as prepared by diamond blade microtomy as described above. This sample was then oriented so that the direction of the incident laser beam is parallel to the original plane of the drop-cast film, as shown in Figure 1b. Heat propagates along the laser beam direction to create a heat flow in the original in-plane direction of the drop-cast film. We measured $\Lambda_\parallel$ at 9.1 MHz using both 10× ($w_0 = 6.7$ μm) and 20× objective lens ($w_0 = 3.4$ μm). Because of the small laser spot size and substrate with low thermal conductivity used in this TDTR measurement, steady-state heating ΔT_{ss} of the probed region of PEDOT film limits the laser power that can be used in the measurement. ΔT_{ss} can be calculated by setting the modulation frequency to zero in the thermal modeling.[14] We set the power of the pump and probe beam accordingly to maintain $\Delta T_{ss} < 30$ K. The largest ΔT_{ss} appears when measuring in-plane thermal conductivity of thick PEDOT films using 20× objective lens. The laser powers are reduced so that the pump and probe power absorbed in the transducer is ≈0.4 mW and ≈0.2 mW, respectively. The corresponding $\Delta T_{ss} \approx 27$ K when the thermal conductivity of PEDOT thick film is ≈0.3 W m^{-1} K^{-1}. Lateral heat spreading in the Al film helps to reduce ΔT_{ss}. Different laser powers were used in the measurements of in-plane thermal conductivity of PEDOT:PSS samples with different DMSO concentrations to maintain the similar ΔT_{ss}. In comparison, the total laser power absorbed in the transducer when measuring spin-cast thin PEDOT films was ≈5 mW, which results in $\Delta T_{ss} \approx 3$ K.

The sensitivity of the data analysis to the interfacial thermal conductance G of the Al-transducer/sample interface is small when the thermal conductivity Λ is low. As shown in Figure 20 of ref 16, the ratio data are much less sensitive to G in comparison to Λ over the range of thermal conductivities ($0.2 < \Lambda < 1$ W m^{-1} K^{-1}). This low sensitivity makes any attempt to fit the interface conductance highly susceptible to systematic errors but also reduces the propagation of errors from uncertainties in G into uncertainties in Λ. The key parameter for determining this error propagation is the ratio of the sensitivities to the two parameters S_G/S_Λ. With decreasing Λ and increasing G, the sensitivity ratio S_G/S_Λ decreases, which reduces the error propagation from the uncertainty in G.

The interfacial thermal conductance can be determined reliably only when the thermal conductivity is high. Wang et al.[15] reported that the interfacial thermal conductance between Al and a polymer fiber with the microtomed interface is $G = 52$ MW m^{-2} K^{-1}. In the data analysis below, we therefore fix the interfacial thermal conductance between PEDOT and the Al transducer at $G = 50$ MW m^{-2} K^{-1}. The error bars on the data points include the error propagation created by a wide range of values for the interfacial thermal conductance $30 < G < 200$ MW m^{-2} K^{-1}. Losego et al.[26] reported $G > 200$ MW m^{-2} K^{-1} for interfaces between Al and extremely thin polymer films. Hsieh et al.[27] also found a negligible effect of interfaces on the effective thermal conductivity of thin PMMA films. (We set the thermal conductance of the PEDOT/substrate interface to $G = 50$ MW m^{-2} K^{-1} but the sensitivity of the data to the PEDOT/Si interface is negligible except for measurements of the thinnest layers at low modulation frequency.)

The error bars of the TDTR measurements can be obtained by taking into account the individual uncertainties and sensitivities of the parameters in the thermal model.[14] When measuring $\Lambda_\parallel$ of drop-cast PEDOT films, higher magnification objective lens (10× and 20×) were used, which results in larger error propagation compared with using 5× objective lens. For example, assuming a 5% uncertainty in beam spot size, errors in measuring thermal conductivity propagated from the uncertainty in the beam spot size are 0.6% using 5×, 2% using 10×, and 10% using 20×, respectively. In addition, the error bars of in-plane thermal conductivity also include the variations from the measurements done by different objective lens and at different locations (at least three locations) on the sample surface, which is why the error bars are larger for in-plane thermal conductivity.

3.3. Elastic Constants. The elastic constants of spin-cast PEDOT films (C_{11} and C_{44}) were measured using pump−probe techniques. C_{11} is calculated from ρv_L^2, where the longitudinal speed of sound $v_L = 2d/t$, where t was measured using the longitudinal acoustic echoes in a TDTR measurement on a ≈60 nm-thick spin-cast PEDOT film; The film density ρ is calculated by determining the film composition and areal density of atoms (atoms per area) in the spin-cast PEDOT thin films using Rutherford backscattering spectrometry (RBS). For

DOI: 10.1021/ma502099t
Macromolecules 2015, 48, 585−591

example, in the 149 ± 5 nm spin-cast PEDOT film (the film thickness is measured by AFM), the areal density of C, S, O, and H atoms is 0.45×10^{18} atoms/cm^2, 0.06×10^{18} atoms/cm^2, 0.16×10^{18} atoms/cm^2, and 0.41×10^{18} atoms/cm^2, respectively, so the film density is 1.2 ± 0.1 g/cm^3.

C_{44} is determined from the velocity of surface acoustic wave (SAW) v_{SAW} measured for a Al(160 nm)/PEDOT(140 nm)/SiO2(315 nm)/Si layered structure. SAW are generated and detected in the pump−probe experiment using an elastomeric phase-shift mask made of PDMS.[28] Conventional PDMS (Sylgard 184, Dow Corning) was cast and cured on a silicon grating mold (700 nm periodicity, 50% duty cycle, and 350 nm groove depth) to make the mask. The mask spatially modulates the incident light intensity of the pump beam, thereby creating a periodic temperature profile and generating SAW. The mask also spatially modulates the sensitivity of the reflected intensity to surface displacements and enables detection of SAW.[28]

We model v_{SAW} of the trilayer structure (Al/PEDOT/SiO_2) numerically using a Green's function method.[29] The inputs to the model are elastic constants, density and thickness of each layer. The Al layer (C_{11} = 108 GPa, C_{12} = 63 GPa, C_{44} = 28.3 GPa, and ρ = 2.7 g/cm^3)[28] is a (111) textured film. The PEDOT film is modeled using two elastic constants, C_{11} and C_{44}. C_{11} of PEDOT film is taken from the measured value on a ≈60 nm-thick film; C_{44} of the PEDOT film is the adjustable parameter in the model. The substrate is treated as an semi-infinite amorphous SiO_2 layer (C_{11} = 78 GPa, C_{44} = 31.6 GPa, ρ = 2.2 g/cm^3).[30,31] C_{44} of the PEDOT film is determined by adjusting C_{44} in the model to make the measurement of v_{SAW} match with the model prediction.

The thicknesses of Al and PEDOT layers in the structure are optimized for the measurement of C_{44}. If the PEDOT film is too thick ($d \gg \lambda$, where λ is the wavelength of SAW), the PDMS mask can drastically affect the wave modes because PDMS and PEDOT have similar elastic constants. If the PEDOT film is too thin, the sensitivity of v_{SAW} to C_{44} is small. A relatively thick Al film (≈160 nm) is needed in the SAW measurement of a thin layer to optimize the sensitivity of v_{SAW} to C_{44}. This is because the SAW velocity is relatively insensitive to elastic constants near the surface and more sensitive to the elastic constants at a depth on the order of $\approx\lambda/\pi$. For a typical optimized geometry in our measurements (Al(160 nm)/PEDOT(140 nm)/SiO2(315 nm)/Si), the sensitivity of v_{SAW} to C_{44} of PEDOT film is ≈0.12.

We validated our approach using an Al/PMMA/Si stack and varied the thickness of the PMMA film between 50 to 450 nm. When the PMMA film is thinner than 200 nm, the measured v_{SAW} agrees with the predicted v_{SAW}.[32] When the PMMA film is thicker than 200 nm, multiple high frequency modes, which are clearly not the SAW of the sample, dominate the signal, indicating the failure of this approach when the polymer layer is thicker than 200 nm.

4. RESULTS AND DISCUSSION

Figure 2 shows the dependence of σ on the DMSO concentration in aqueous solution for drop-cast and spin-cast PEDOT films. Adding cosolvent DMSO significantly increases σ, which is believed to act as a structural dopant for changes in the film morphology.[33−37] In the PEDOT:PSS aqueous solution, the PEDOT molecules are bound to the PSS chains by ionic interactions and form core−shell micelles with a PEDOT-rich core and a PSS-rich shell.[34,37] The addition of a high boiling-point polar solvent is thought to enable the

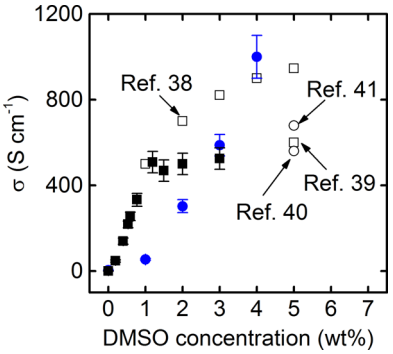

Figure 2. In-plane electrical conductivity σ, measured by a four-point probe as a function of DMSO concentration in aqueous solution for drop-cast (black filled squares) and spin-cast (blue filled dots) PEDOT:PSS films. For comparison, we include σ measured on 3−10 μm-thick DMSO-mixed PEDOT:PSS films from ref 38: (open squares) σ reported in ref 39 for 5−8 μm-thick films prepared using 5 wt % DMSO (open squares); σ for spin-cast 120 nm-thick films from ref 40 (open circles); and σ for a spin-cast 130 nm-thick film from ref 41 (open circles).

reorganization of the conducting PEDOT molecules and the insulating PSS chains, leading to an interconnected network of elongated, densely packed, reoriented PEDOT molecules.[33−37]

However, the increase of σ with DMSO concentration in drop-cast and spin-cast PEDOT films has different trends. In the drop-cast films, σ increases rapidly from ≈0 to ≈500 S cm^{-1} when adding 0−1.2 wt % DMSO in the PEDOT:PSS solution and reaches a plateau with additional DMSO. The maximum electrical conductivity we obtained is lower than 945 S cm^{-1} on 3−10 μm drop-cast PEDOT films reported by Zhang et al.[38] and ≈600 S cm^{-1} on 5−8 μm drop-cast PEDOT films reported by Kuryak[39] using the same PEDOT:PSS solution (Clevious PH1000) and same DMSO concentration. Their drop-cast samples were made by first keeping the sample on a hot plate at 50 °C for a certain time (1 h in ref 38 and 4 h in ref 39) and then 120 °C for 15 min. In the spin-cast films, σ increases gradually from ≈0 to ≈1000 S cm^{-1} with increasing the DMSO concentration from 0 to 4 wt %. This conductivity is higher than the reported value 560 S cm^{-1} on spin-cast 120 nm-thick PEDOT film on glass substrate (spin-casting at a speed of 1500 rpm for 40 s and then 2000 rpm for 20 s) from Gasiorowski et al.[40] and 680 S cm^{-1} on spin-cast 130 nm-thick PEDOT film on glass substrate (spin-casting at a speed of 1000 rpm for 40 s and annealing at 120 °C for 30 min) from Zhou et al.[41] using the same solution.

We do not yet understand why electrical conductivity in films prepared by drop-cast and spin-cast with the same DMSO concentration is different. One possible reason is the different combinations of evaporation temperature and time used in preparing the drop-cast and spin-cast films, which will alter the molecular-scale kinetics that determines the polymer morphology. The evaporation temperature has been previously shown to affect the electrical conductivity of DMSO-mixed PEDOT:PSS films.[42,43]

For the TDTR measurement of thermal conductivity and heat capacity of spin-cast PEDOT films, we define a parameter ξ, as in our previous work in measuring organic thin films,[19] to quantify the goodness-of-fit. ξ is the sum of the standard deviation between the model prediction and measurement data at all three frequencies and delay times from 0.1 to 4 ns. Figure 3a shows the contour of constant $\xi = 2\xi_{min}$ (i.e., a 95%

DOI: 10.1021/ma502099t
Macromolecules 2015, 48, 585−591

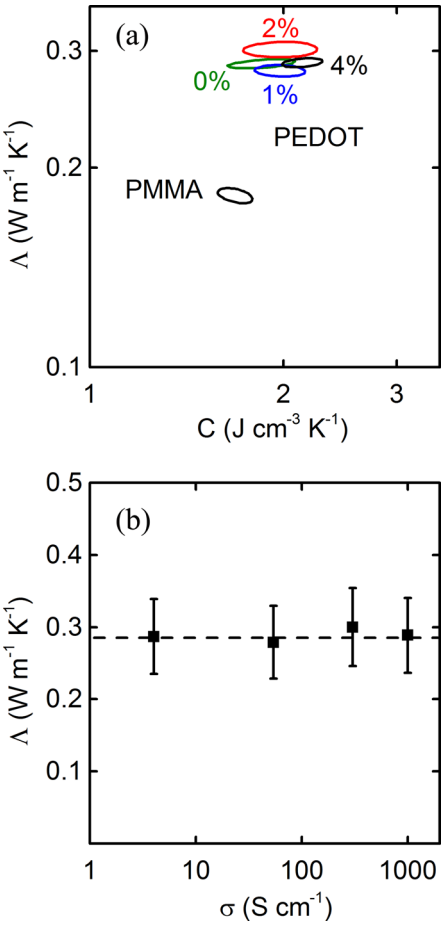

Figure 3. (a) Contour map derived from the goodness-of-fit for frequency-dependent TDTR data as a function of thermal conductivity Λ and heat capacity C for ≈65 nm-thick spin-cast DMSO-mixed PEDOT:PSS films with different DMSO compositions (0–4 wt % DMSO; 0%, green; 1%, blue; 2%, red; and 4%, black), measured at ≈300 K. The contour for a validation measurement of a ≈100 nm-thick PMMA sample is also shown. The contour lines represent 95% confidence level that the true values of Λ and C fall within the contour. (b) Λ as a function of in-plane electrical conductivity σ of spin-cast DMSO-mixed PEDOT:PSS films. The dashed lines are the average values Λ = 0.29 W m^{-1} K^{-1}. The uncertainties of σ are smaller than the size of the data symbols.

confidence level) as a function of Λ and C of ≈100 nm PMMA thin film and PEDOT spin-cast thin films. These uncertainties are determined by the signal-to-noise ratio of the measurement and the quality of the fit of the data to the thermal model. The total uncertainties of the measured Λ and C are calculated by adding these measurement uncertainties in quadrature with the systematic errors that propagate from uncertainties in the film thickness, laser spot size, and thermal properties of the transducer film and substrate. The best fits are Λ = 0.29 ± 0.05 W m^{-1} K^{-1} and C = 2.0 ± 0.4 J cm^{-3} K^{-1} for spin-cast PEDOT films with different DMSO compositions. We do not observe a significant change in either Λ or C with different DMSO compositions within our measurement accuracy, as shown in Figure 3b.

Figure 4 shows elastic constants (C_{11} and C_{44}) as a function of in-plane electrical conductivity σ of spin-cast PEDOT films. The error bars of the measured elastic constants are calculated by considering error propagation from experimental uncertainties, such as the uncertainty from the measured v_{SAW} and film

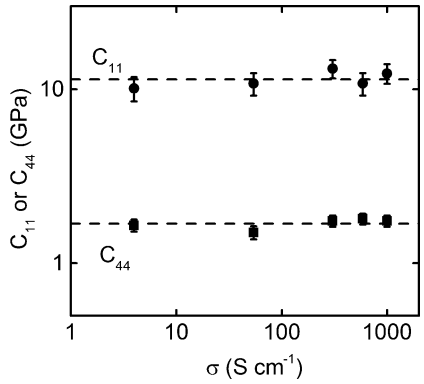

Figure 4. Elastic constants C_{11} (dots) and C_{44} (squares) as a function of in-plane electrical conductivity σ of spin-cast DMSO-mixed PEDOT:PSS films. C_{11} is measured by picosecond acoustics; C_{44} is measured by velocity of surface acoustic waves. The dashed lines are the average values C_{11} ≈ 11 GPa and C_{44} ≈ 1.7 GPa. The uncertainties of σ are smaller than the size of the data symbols.

thickness. Both C_{11} and C_{44} of spin-cast PEDOT films are independent of DMSO compositions within the uncertainty of our measurements. We find C_{11} ≈ 11 GPa and C_{44} ≈ 1.7 GPa.

These measurements of the elastic constants and through-plane thermal conductivity of spin-cast PEDOT films support our assumption that the phonon contribution to thermal conductivity in PEDOT films does not change significantly with DMSO composition.

Figure 5 shows $\Lambda_\perp$ and $\Lambda_\parallel$ of drop-cast PEDOT films as a function of σ. $\Lambda_\perp$ of the drop-cast layers does not change with σ

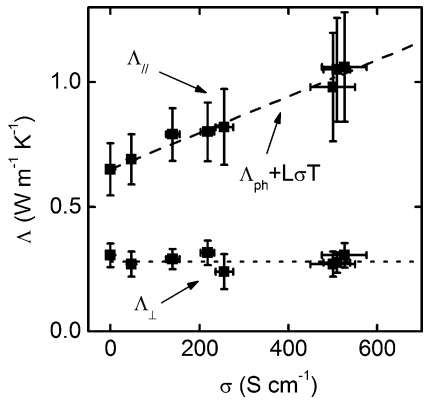

Figure 5. Through-plane ($\Lambda_\perp$, fill circles) and in-plane ($\Lambda_\parallel$, filled squares) thermal conductivity of drop-cast DMSO-mixed PEDOT:PSS films measured by TDTR as a function of in-plane electrical conductivity σ, measured at ≈325 K. $\Lambda_\perp$ of the drop-cast DMSO-mixed PEDOT:PSS films does not change with σ (dot line is the average value $\Lambda_\perp$ ≈ 0.3 W m^{-1} K^{-1}). $\Lambda_\parallel$ of drop-cast DMSO-mixed PEDOT:PSS film increases from $\Lambda_\parallel \approx 2\Lambda_\perp$ for the pristine film to $\Lambda_\parallel \approx 3\Lambda_\perp$ for the DMSO-mixed film with the highest electrical conductivity. The Wiedemann–Franz law and Sommerfeld value of Lorenz number L, plotted as a dashed line ($\Lambda_\parallel = \Lambda_{ph} + L\sigma T$), is consistent with the variation of $\Lambda_\parallel$ on σ assuming the phonon contribution to thermal conductivity Λ_{ph} is constant.

and is consistent with $\Lambda_\perp$ measured on spin-cast films. Thermal conductivity of the drop-cast PEDOT film is anisotropic with $\Lambda_\parallel \approx 2\Lambda_\perp$ when the PEDOT film is not electrically conductive. This result suggests that even in the absence of DMSO, the molecular alignment created during the evaporation process has a preferred direction parallel to the film surface. The anisotropy

DOI: 10.1021/ma502099t
Macromolecules 2015, 48, 585–591

in the thermal conductivity increases with increasing in-plane electrical conductivity, reaching $\Lambda_{\parallel} \approx 3\Lambda_{\perp}$ for the samples with the highest in-plane electrical conductivity.

We relate the increase in $\Lambda_{\parallel}$ of drop-cast PEDOT films as a function of electrical conductivity to the estimated electronic component of the thermal conductivity using the WFL and the Sommerfeld value of the Lorenz number, $\Lambda_{\parallel} = \Lambda_{ph} + L\sigma T$;[7] we assume that the phonon component of the thermal conductivity Λ_{ph} is constant. This relationship is plotted in Figure 5 as dashed line. Our data are consistent with these assumptions. If we further assume that the Sommerfeld value of the Lorenz number also applies in the through-thickness direction, then we conclude that the through thickness electrical conductivity is much smaller than the in-plane electrical conductivity.

Kim et al.[4] measured the anisotropic thermal conductivity of ≈1.4 μm-thick spin-cast DMSO-mixed PEDOT:PSS film and found $\Lambda_{\parallel} = 0.42 \pm 0.07$ W m^{-1} K^{-1} and $\Lambda_{\perp} = 0.30 \pm 0.02$ W m^{-1} K^{-1} when $\sigma \approx 620$ S cm^{-1}, which suggests an anomalously small value of L. Our data for drop-cast layers extrapolates to $\Lambda_{\parallel} \approx 1.1$ W m^{-1} K^{-1} at this electrical conductivity, a factor of 2.5 higher than reported by Kim et al.[4] If we use our measurements of thermal conductivity and the power factors σS^2 reported in ref 4, we estimate that the maximum ZT at room temperature of highly conducting PEDOT:PSS is ZT ≈ 0.11 at a conductivity of $\sigma \approx 900$ S cm^{-1}.

Note: while our paper was under review, a closely related paper by Wei et al.[44] was published. They demonstrated the anisotropic electrical conductivity and thermal conductivity of PEDOT: PSS films treated with 3 wt % ethylene glycol ($\sigma_{\perp} \approx 36$ S cm^{-1}, $\sigma_{\parallel} \approx 820$ S cm^{-1}).$\Lambda_{\perp} = 0.15 \pm 0.04$ W m^{-1} K^{-1} and $\Lambda_{\parallel} = 0.84 \pm 0.33$ W m^{-1} K^{-1}, which was measured on 100 μm and 3.5 mm-thick PEDOT: PSS films, respectively. They attribute the observed anisotropic thermal conductivity to the lattice contribution from PSS due to a more parallel-to-substrate chain orientation.

5. SUMMARY

We find that thermal conductivity of drop-cast DMSO-mixed PEDOT:PSS films is highly anisotropic when the electrical conductivity is large, in part due to a significant electronic contribution to the in-plane thermal conductivity. The changes of thermal conductivity as a function of electrical conductivity data are consistent with the Wiedemann–Franz law and the Sommerfeld value of the Lorenz number. Measurements of the elastic constants and through-plane thermal conductivity of spin-cast DMSO-mixed PEDOT:PSS films support the assumption that the phonon contribution to thermal conductivity does not change significantly with DMSO composition.

AUTHOR INFORMATION

Corresponding Author

*(J.L.) E-mail: junliu@illinois.edu.

Present Address

#Currently at the California Maritime Academy, Vallejo, California 94590.

Notes

The authors declare no competing financial interest.

ACKNOWLEDGMENTS

Thermal conductivity measurements were supported by AFOSR MURI FA9550-12-1-0002. Development and application of SAW measurements to thin polymer films was supported by the International Institute for Carbon Neutral Energy Research (WPI-I2CNER sponsored by the World Premier International Research Center Initiative (WPI), MEXT, Japan. TDTR measurements were done using the equipment in the Laser Facility of the Frederick Seitz Materials Research Laboratory (MRL) at the University of Illinois at Urbana–Champaign (UIUC). Diamond blade ultramicrotomy was done in the Center for Microanalysis of Materials (CMM) of the MRL at UIUC. Work at the Molecular Foundry was supported by the Office of Science, Office of Basic Energy Sciences, of the U.S. Department of Energy under Contract No. DE-AC02-05CH11231.

REFERENCES

(1) Groenendaal, L.; Jonas, F.; Freitag, D.; Pielartzik, H.; Reynolds, J. R. *Adv. Mater.* **2000**, *12*, 481–494.
(2) Wang, Y. *J. Phys: Conf. Ser.* **2009**, *152*, 012023.
(3) Bubnova, O.; Khan, Z. U.; Malti, A.; Braun, S.; Fahlman, M.; Berggren, M.; Crispin, X. *Nat. Mater.* **2011**, *10*, 429–433.
(4) Kim, G. H.; Shao, L.; Zhang, K.; Pipe, K. P. *Nat. Mater.* **2013**, *12*, 719–723.
(5) Goldsmid, H. J. *Electronic Refrigeration*; Pion: London, 1986.
(6) Franz, R.; Wiedemann, G. *Ann. Phys.* **1853**, *15*, 497–531.
(7) Kittel, C. *Introduction to Solid State Physics*, 8th ed.; Wiley: New York, 2004.
(8) Jeong, C.; Kim, R.; Lundstrom, M. S. *J. Appl. Phys.* **2012**, *111*, 113707.
(9) Bian, Z.; Zebarjadi, M.; Singh, R.; Ezzahri, Y.; Shakouri, A.; Zeng, G.; Bahk, J. H.; Bowers, J. E.; Zide, J. M. O.; Gossard, A. C. *Phys. Rev. B* **2007**, *76*, 205311.
(10) Zhang, X.; Zhang, Q.-G.; Cao, B.-Y.; Fujii, M.; Takahashi, K.; Ikuta, T. *Chin. Phys. Lett.* **2006**, *23*, 936.
(11) Volklein, F.; Reith, H.; Cornelius, T. W.; Rauber, M.; Neumann, R. *Nanotechnology* **2009**, *20*, 325706.
(12) Salamon, M. B.; Bray, J. W.; DePasquali, G.; Craven, R. A.; Stucky, G.; Schultz, A. *Phys. Rev. B* **1975**, *11*, 619–622.
(13) Mermilliod, N.; Zuppiroli, L.; Francois, B. *J. Phys. (Paris)* **1980**, *41*, 1453–1458.
(14) Cahill, D. G. *Rev. Sci. Instrum.* **2004**, *75*, 5119–5122.
(15) Wang, X.; Ho, V.; Segalman, R. A.; Cahill, D. G. *Macromolecules* **2013**, *46*, 4937–4943.
(16) Cahill, D. G.; Braun, P. V.; Chen, G.; Clarke, D. R.; Fan, S.; Goodson, K. E.; Keblinski, P.; King, W. P.; Mahan, G. D.; Majumdar, A.; Maris, H. J.; Phillpot, S. R.; Pop, E.; Shi, L. *Appl. Phys. Rev.* **2014**, *1*, 011305.
(17) *Springer Handbook of Electronic and Photonic Materials*; Safa, K., Peter, C., Eds.; Springer Science and Business Media, Inc.: Berlin, 2007.
(18) Liu, J.; Zhu, J.; Tian, M.; Gu, X.; Schmidt, A.; Yang, R. *Rev. Sci. Instrum.* **2013**, *84*, 034902.
(19) Wang, X.; Liman, C. D.; Treat, N. D.; Chabinyc, M. L.; Cahill, D. G. *Phys. Rev. B* **2013**, *88*, 075310.
(20) Wei, C.; Zheng, X.; Cahill, D. G.; Zhao, J.-C. *Rev. Sci. Instrum.* **2013**, *84*, 071301–9.
(21) Ditmars, D. A.; Plint, C. A.; Shukla, R. C. *Int. J. Thermophys.* **1985**, *6*, 499–515.
(22) *Silicon (Si), Debye temperature, heat capacity, density, hardness, melting point*; Madelung, O.; Rössler, U.; Schulz, M., Eds.; Springer-Verlag: Berlin, 2002; Vol. *41A1b*.
(23) Cahill, D. G.; Watanabe, F. *Phys. Rev. B* **2004**, *70*, 235322.
(24) Putnam, S. A.; Cahill, D. G.; Ash, B. J.; Schadler, L. S. *J. Appl. Phys.* **2003**, *94*, 6785–6788.

DOI: 10.1021/ma502099t
Macromolecules 2015, 48, 585–591

(25) Assael, M. J.; Botsios, S.; Gialou, K.; Metaxa, I. N. *Int. J. Thermophys.* **2005**, *26*, 1595−1605.
(26) Losego, M. D.; Moh, L.; Arpin, K. A.; Cahill, D. G.; Braun, P. V. *Appl. Phys. Lett.* **2010**, *97*, 011908.
(27) Hsieh, W. P.; Losego, M. D.; Braun, P. V.; Shenogin, S.; Keblinski, P.; Cahill, D. G. *Phys. Rev. B* **2011**, *83*, 174205.
(28) Li, D.; Zhao, P.; Zhao, J.-C.; Cahill, D. G. *J. Appl. Phys.* **2013**, *114*, 143102.
(29) Zhang, X.; Comins, J. D.; Every, A. G.; Stoddart, P. R.; Pang, W.; Derry, T. E. *Phys. Rev. B* **1998**, *58*, 13677−13685.
(30) McSkimin, H. J. *J. Appl. Phys.* **1953**, *24*, 988−997.
(31) Bogardus, E. H. *J. Appl. Phys.* **1965**, *36*, 2504−2513.
(32) Zhang, X.; Gan, C.; Fei, D.; Zhang, S. *J. Phys. IV France* **1994**, *04*, C7−725−C7−728.
(33) Crispin, X.; Jakobsson, F. L. E.; Crispin, A.; Grim, P. C. M.; Andersson, P.; Volodin, A.; van Haesendonck, C.; Van der Auweraer, M.; Salaneck, W. R.; Berggren, M. *Chem. Mater.* **2006**, *18*, 4354−4360.
(34) Alemu Mengistie, D.; Wang, P.-C.; Chu, C.-W. *J. Mater. Chem. A* **2013**, *1*, 9907−9915.
(35) van de Ruit, K.; Cohen, R. I.; Bollen, D.; van Mol, T.; Yerushalmi-Rozen, R.; Janssen, R. A. J.; Kemerink, M. *Adv. Funct. Mater.* **2013**, *23*, 5778−5786.
(36) Wei, Q.; Mukaida, M.; Naitoh, Y.; Ishida, T. *Adv. Mater.* **2013**, *25*, 2831−2836.
(37) Palumbiny, C. M.; Heller, C.; Schaffer, C. J.; Korstgens, V.; Santoro, G.; Roth, S. V.; Muller-Buschbaum, P. *J. Phys. Chem. C* **2014**, *118*, 13598−13606.
(38) Zhang, B.; Sun, J.; Katz, H. E.; Fang, F.; Opila, R. L. *ACS Appl. Mater. Interfaces* **2010**, *2*, 3170−3178.
(39) Kuryak, C. A. *Nanostructured Thin Film Thermoelectric Composite Materials Using Conductive Polymer PEDOT:PSS*, Master's Thesis, Massachusetts Institute of Technology: Cambridge, MA, 2013.
(40) Gasiorowski, J.; Menon, R.; Hingerl, K.; Dachev, M.; Sariciftci, N. S. *Thin Solid Films* **2013**, *536*, 211−215.
(41) Zhou, Y.; Cheun, H.; Choi, S.; Potscavage, W. J.; Fuentes-Hernandez, C.; Kippelen, B. *Appl. Phys. Lett.* **2010**, *97*, 153304.
(42) Na, S.-I.; Wang, G.; Kim, S.-S.; Kim, T.-W.; Oh, S.-H.; Yu, B.-K.; Lee, T.; Kim, D.-Y. *J. Mater. Chem.* **2009**, *19*, 9045−9053.
(43) Wang, G.-F.; Tao, X.-M.; Xin, J. H.; Fei, B. *Nanoscale Res. Lett.* **2009**, *4*, 613.
(44) Wei, Q.; Mukaida, M.; Kirihara, K.; Ishida, T. *ACS Macro Lett.* **2014**, *3*, 948−952.

DOI: 10.1021/ma502099t
Macromolecules 2015, 48, 585−591